Scientific Research Publishing

International Journal of Astronomy and Astrophysics, 2026, 16(1), 25-40
https://www.scirp.org/journal/ijaa
ISSN Online: 2161-4725
ISSN Print: 2161-4717

Warm Dark Matter Properties from Dwarf Spheroidal Galaxy Observations

Bruce Hoeneisen

Universidad San Francisco de Quito, Quito, Ecuador
Email: bhoeneisen@usfq.edu.ec

How to cite this paper: Hoeneisen, B. (2026) Warm Dark Matter Properties from Dwarf Spheroidal Galaxy Observations. *International Journal of Astronomy and Astrophysics*, **16**, 25-40.
https://doi.org/10.4236/ijaa.2026.161003

Received: December 30, 2025
Accepted: March 9, 2026
Published: March 12, 2026

Abstract

Most matter in the Universe is in a "dark matter" form that has only been observed through its gravitational interaction. How warm is this dark matter? A new constraint has become available thanks to the observations of the line-of-sight velocities of individual stars in dwarf spheroidal galaxies dSph, which allow a measurement of the dark matter density $\rho_h(r)$. From the measured $\rho_h(r)$ of 27 dwarf spheroidal galaxies dSph, we obtain an estimate of the comoving thermal velocity and mass of the dark matter particles.

Keywords

Warm Dark Matter, Spheroidal Galaxies, Dwarf Galaxies, Free Streaming, Dark Matter

1. Introduction

Most matter in the Universe is in a "dark matter" form that has only been observed through its gravitational interaction. How warm is this dark matter? Recent measurements of the dark matter density $\rho_h(r)$ of dwarf spheroidal galaxies dSph present a new opportunity to answer this question [1]-[6]. The "warmness" of dark matter can be specified by the comoving dark matter root-mean-square thermal velocity $v_{h\mathrm{rms}}(1)$. Previously, we have presented studies of $v_{h\mathrm{rms}}(1)$ with the rotation curves of dwarf [7] and spiral [8] [9] galaxies, and with the density runs of elliptical galaxies [10]. Redundant measurements of $v_{h\mathrm{rms}}(1)$ are needed to gain confidence in the assumptions. Obtaining $\rho_h(r)$ of dwarf spheroidal galaxies dSph with little rotation has become possible with the observation of the line-of-sight velocities of individual stars. In the present analysis, we estimate $v_{h\mathrm{rms}}(1)$ from the measured dark matter density of 27 (mostly) dwarf spheroidal galaxies dSph. The special interest in dwarf spheroidal galaxies dSph is their higher

mass-to-light ratio, lower rotation velocity, and their possible belonging to the first generation of galaxies in the warm dark matter scenario, which makes them complementary to other measurements.

In Section 2, we define $v_{h\mathrm{rms}}(1)$, and the related linear density power spectrum cut-off wavevector k_{fs} and "standard thermal relic mass" m_{th}, and explain the measurement method. In Section 3, we present the measurements and results. Similar estimates are obtained from dwarf galaxies in the Local Field in Section 4. A discussion of the present and previous measurements of $v_{h\mathrm{rms}}(1)$ is presented in Section 5. Conclusions follow.

2. Warm Dark Matter

We assume dark matter is a non-relativistic, non-degenerate gas of particles of mass m_h that are collisionless, or have elastic collisions. Let $v_{h\mathrm{rms}}(a)$ be the root-mean-square thermal velocity of the dark matter particles in the early, nearly homogeneous, Universe at expansion parameter a (normalized to $a(t_0)=1$ at the present time t_0). $v_{h\mathrm{rms}}(a)$ scales as a^{-1}, while the dark matter density $\rho_h(a)\propto a^{-3}$, so

$$v_{h\mathrm{rms}}(1)=v_{h\mathrm{rms}}(a)\left(\frac{\Omega_c\rho_{\mathrm{crit}}}{\rho_h(a)}\right)^{1/3} \tag{1}$$

is an adiabatic invariant. Consider an observer at the peak of a density perturbation in the early Universe. As the Universe expands, this observer "sees" dark matter expand, reach maximum expansion, and then collapse to form the core of a galaxy. If the expansion and contraction were adiabatic, then $v_{h\mathrm{rms}}(1)=v'_{h\mathrm{rms}}(1)$ with

$$v'_{h\mathrm{rms}}(1)\equiv\sqrt{3\left\langle v_{rh}^2\right\rangle}\left(\frac{\Omega_c\rho_{\mathrm{crit}}}{\rho_h(r_{\mathrm{min}})}\right)^{1/3}, \tag{2}$$

if dark matter is collisional. $\sqrt{\left\langle v_{rh}^2\right\rangle}$ is the root-mean-square of the radial component of the velocity of the dark matter particles, and $\rho_h(r_{\mathrm{min}})$ is the galaxy core dark matter density.

In general,

$$v_{h\mathrm{rms}}(1)=v'_{h\mathrm{rms}}(1)\frac{\epsilon}{f}. \tag{3}$$

If there is no relaxation, $\epsilon=1$. Due to relaxation, $\epsilon<1$. If dark matter is collisional, $f=1$. If dark matter is collisionless, so the dark matter particle velocities are mostly radial, then $f\approx\sqrt{3}$ [9].

The free-streaming of dark matter particles into, or out of, density minimums, or maximums, attenuates the linear comoving density power spectrum $P_{\Lambda\mathrm{CDM}}(k)$ of the cold dark matter ΛCDM cosmology by a factor $\tau^2(k)$. k is the comoving wavevector. For a Maxwell distribution of velocities, the attenuation factor has the form $\tau^2(k)=\exp\left(-k^2/k_{\mathrm{fs}}^2\right)$ [11], which defines our free-streaming cut-off

wavevector k_{fs} (other definitions in the literature are $\tau^2(k_{\mathrm{fs}}) = 1/2$ or 1/4). For a Maxwell distribution of velocities, the relation between $v_{h\mathrm{rms}}(1)$ and k_{fs} is [11] [12].

$$k_{\mathrm{fs}} = 0.88\sqrt{\frac{4\pi G\Omega_m \rho_{\mathrm{crit}} a_{\mathrm{eq}}}{v_{h\mathrm{rms}}^2(1)}} = 1.41\,\mathrm{Mpc}^{-1}\frac{493\ \mathrm{m/s}}{v_{h\mathrm{rms}}(1)}. \tag{4}$$

Limits on k_{fs} in the literature are often expressed as limits on the "standard thermal relic mass" m_{th} defined by Equation (6) and Equation (7) of [13]. Note however that the actual dark matter particle mass m_h is model-dependent (see [14] or **Appendix E**). The expansion parameter at which dark matter becomes non-relativistic can be defined as $a_{\mathrm{NR}} \equiv v_{h\mathrm{rms}}(1)/c$.

In summary, the "warmness" of dark matter can be described by any one of the equivalent parameters $v_{h\mathrm{rms}}(1)$, k_{fs}, m_{th}, m_h or a_{NR}.

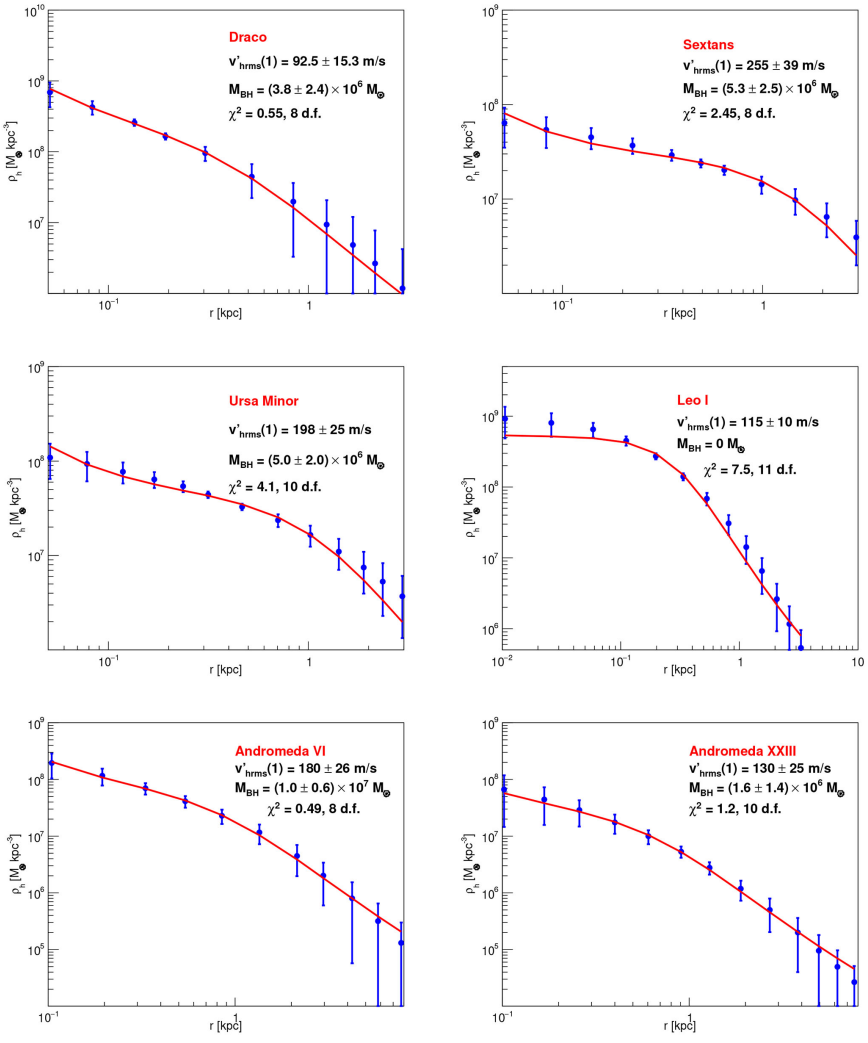

Figure 1. Dark matter densities $\rho_h(r)$ of dwarf spheroidal dSph galaxies. The data are from [1] for Draco, Sextans and Ursa Minor, [2] for Leo I, and [3] for Andromeda VI and Andromeda XXIII. The uncertainties (that have been symmetrized) are 1σ. The fits are integrations of hydrostatic Equations (5) as explained in the text.

Table 1. For some dwarf spheroidal galaxies dSph, we present the stellar mass M_*, neutral hydrogen mass $M_{\rm HI}$, Wolf dynamical mass up to the half-light radius $r_{1/2}$: $M_{\rm dyn}(r_{1/2}) \equiv 930\sigma^2 r_{1/2}$, dark matter mass up to the last measured radius $M_h(r_{\rm max})$, and $r_{1/2}$. The data is from the Local Volume Database [15], or [2], except $M_h(r_{\rm max})$ from the fit. Note that these dwarf galaxies are dominated by dark matter down to at least $r = r_{1/2}$. Some entries are not available.

Dwarf	$\log_{10} M_*/M_\odot$	$\log_{10} M_{\rm HI}/M_\odot$	$\log_{10} M_{\rm dyn}/M_\odot$ to $r_{1/2}$	$\log_{10} M_{\rm h}/M_\odot$ to $r_{\rm max}$	$r_{1/2}$ [pc]
Draco	5.78		7.17	8.5	193
Sextans	7.93	7.87		8.8	920
Ursa Minor	5.78		7.24	8.7	250
Leo I	6.96		7.25	8.6	229
Andromeda VI	6.75		7.81	9.1	399
Andromeda XXIII	6.14		7.58	8.5	896
Andromeda XXI	5.81		7.39	8.1	730
Andromeda XXV	5.87		6.85	7.7	562
Aquarius	6.42	6.54	7.26	9.0	320
Sculptor	6.54		7.24	8.6	223
WLM	7.98	7.84	8.36	9.7	799

3. Measurement of $v'_{h\rm rms}(1)$

Some parameters of some dwarf spheroidal galaxies dSph are presented in **Table 1**. We note that the dark matter density dominates even when averaged up to the half-light-radius $r_{1/2}$. The baryon density may dominate at very small r in Leo I.

The measurements of $v'_{h\rm rms}(1)$ are presented in **Figures 1-5**. The sources of the data are cited in the figure captions. The dark matter densities $\rho_h(r)$ are obtained, in the cited references, from the observed line-of-sight stellar velocities of individual stars, with the dynamical Jeans modeling tools *GravSphere* or *JAM*. To perform the fits in **Figures 1-5** with *Minuit*, we have symmetrized the uncertainties, *i.e.*, $\sigma_i = \left(\rho_{h\max}(r_i) - \rho_{h\min}(r_i)\right)/2$. The fits are solutions of the dark-matter-only hydrostatic equations for warm dark matter

$$\nabla \cdot \boldsymbol{g} = -4\pi G\rho_h, \quad \nabla\left(\left\langle v_{rh}^2\right\rangle \rho_h\right) = \rho_h \boldsymbol{g}(1-\kappa_h), \tag{5}$$

see **Appendix A**. The factor $(1-\kappa_h)$ describes rotation of dark matter in the equatorial plane ($\kappa_h = 0$ for no rotation, $\kappa_h \to 1$ for maximum rotation). For the dwarf spheroidal galaxies dSph, we will neglect dark matter rotation, *i.e.* set $\kappa_h = 0$ (but not for rotating irregular dwarfs dIrr, nor for spiral galaxies). We assume that the radial component of the dark matter thermal velocity $\sqrt{\left\langle v_{rh}^2\right\rangle}$ is approximately independent of the radial coordinate r, as justified by the excellent fits, and for reasons explained in [16] and [17], and confirmed for baryons by observations in Figure 2 of [2]. Equations (5) are justified by their excellent fits to

the data, see Figures 1-5. Note that to understand galaxy halos, we need to assume dark matter is warm, *i.e.* $\sqrt{\langle v_{rh}^2 \rangle} > 0$, else we have no Equations (5) to integrate. Let us mention that Equations (5) also describe the rotating Earth atmosphere in the equatorial plane in the approximation of constant temperature. The boundary parameters that are varied to minimize the χ^2 between the measured and calculated dark matter densities $\rho_h(r_i)$, are $\rho_h(r_{\min})$, $v'_{hrms}(1)/\sqrt{1-\kappa_h}$ (with $v'_{hrms}(1)$ defined in (2)), and the mass M_{BH} of a possible central black hole. The effect of baryons in Leo I is studied in **Appendix B**. The fits obtain the dark matter mass $M_h(r_{\max})$ up to the last measured radius r, which turns out to be much larger than the baryonic mass, as shown in Table 1. Baryonic mass is generally less than the dark matter mass, even for $r < r_{1/2}$, but may dominate at smaller r in Leo I.

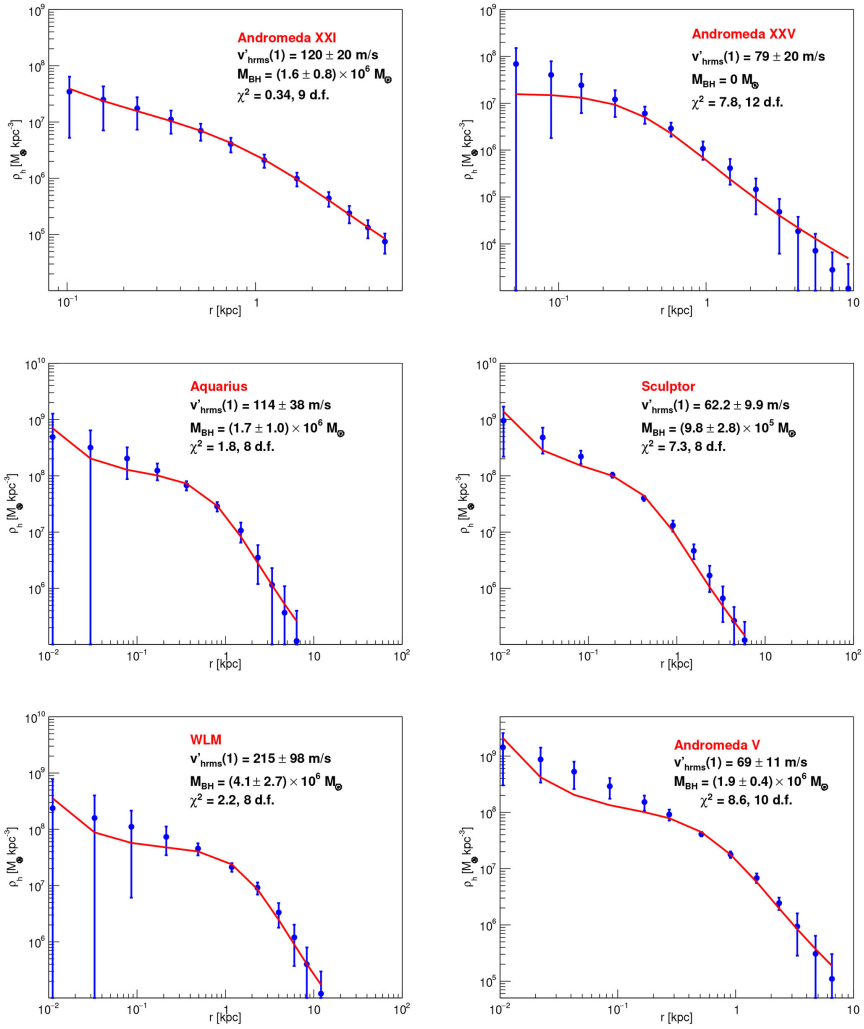

Figure 2. Dark matter densities $\rho_h(r)$ of (mostly) dwarf spheroidal dSph galaxies. The uncertainties (that have been symmetrized) are 1σ. The fits are integrations of hydrostatic Equations (5) as explained in the text. Data from [4] for Andromeda XXI, [5] for Andromeda XXV, [6] for Aquarius, Sculptor and WLM, and from link given in [6] for Andromeda V.

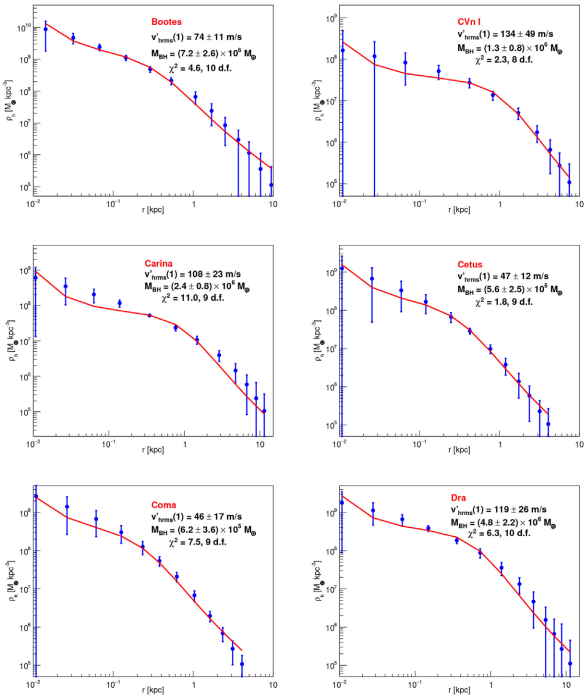

Figure 3. Dark matter densities $\rho_h(r)$ of (mostly) dwarf spheroidal dSph galaxies. The uncertainties (that have been symmetrized) are 1σ. The fits are integrations of hydrostatic Equations (5) as explained in the text. Data from the link https://github.com/koreshk/Estimation-of-phase-space-density-in-dwarf-galaxies on 30 January 2026, given in [6].

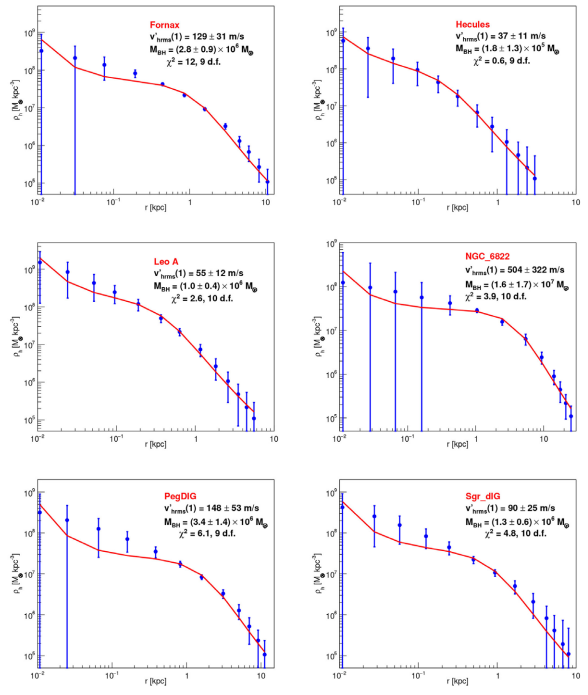

Figure 4. Dark matter densities $\rho_h(r)$ of (mostly) dwarf spheroidal dSph galaxies. The uncertainties (that have been symmetrized) are 1σ. The fits are integrations of hydrostatic Equations (5) as explained in the text. Data from the link given in [6].

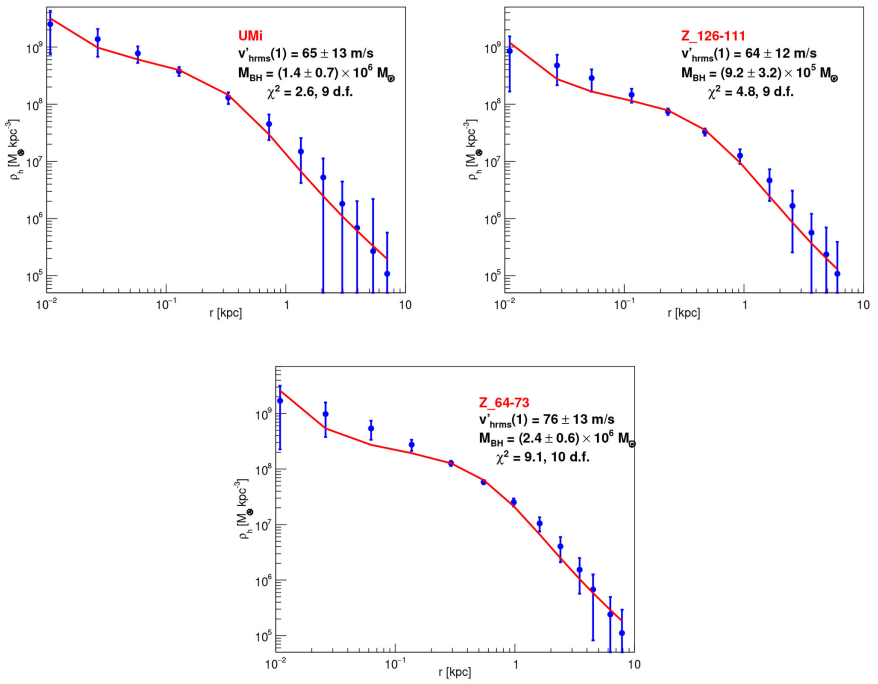

Figure 5. Dark matter densities $\rho_h(r)$ of (mostly) dwarf spheroidal dSph galaxies. The uncertainties (that have been symmetrized) are 1σ. The fits are integrations of hydrostatic Equations (5) as explained in the text. Data from the link given in [6].

4. Dwarf Galaxies in the Local Field

Let us compare the preceding measurements with dwarf spheroidal galaxies dSph, which are generally satellites of the Milky Way or Andromeda, with isolated dwarf galaxies in the Local Field, *i.e.* within 3 Mpc of the Milky Way, excluding Milky Way or Andromeda satellites, see [15]. Thirteen dwarf galaxies in the Local Field have a measured line-of-sight stellar velocity standard deviation *vlos_sigma* that we denote σ_{v1D}. Among these 13 dwarf galaxies, only one (Antilla B) has a host (NGC 3109). These dwarfs may be first-generation galaxies in the warm dark matter scenario. Dark matter density runs are generally not yet measured, so we will make the following approximate assignments of baryon observables to dark matter properties (that we expect to be correct within about a factor 2):

$$r_c \approx r_{1/2} \quad \text{and} \quad \sqrt{\langle v_{rh}^2 \rangle} \approx \sigma_{v1D}. \tag{6}$$

$$\rho_h(r) = \frac{\langle v_{rh}^2 \rangle}{2\pi G r^2} \quad \text{and} \quad r_c \equiv \sqrt{\frac{\langle v_{rh}^2 \rangle}{2\pi G \rho_{ch}}} \tag{7}$$

are the density at large $r \gg r_c$, and the core radius r_c, of a cored isothermal sphere. ρ_{ch} is the core density. Then $v'_{hrms}(1)$ of (2) can be written as

$$v'_{hrms}(1) = \sqrt{3}\left(2\pi G \Omega_c \rho_{crit}\right)^{1/3} \langle v_{rh}^2 \rangle^{1/6} r_c^{2/3}, \tag{8}$$

if dark matter rotation is negligible. From data in the *Local Volume Database* (LVDB) catalog [15], we then obtain the results presented in **Table 2**. We note that several dwarfs in **Table 2** have $v'_{hrms}(1)$ in agreement with the measurements

presented in Figures 1-5. These dwarfs and the dSph reinforce the assumption that they may be first-generation galaxies in the warm dark matter scenario, with little rotation or relaxation.

Table 2. Estimates of $v'_{h\mathrm{rms}}(1)$ from (8) and core dark matter density ρ_{ch} from (7) for all Local Field dwarf galaxies in the LVDB catalog [15] that have a measurement of $\sigma_{v1\mathrm{D}}$ and $M_{\mathrm{dyn}}(r_{1/2})$, assuming the assignments (6). Uncertainties are statistical only. These $v'_{h\mathrm{rms}}(1)$ and ρ_{ch} are only valid if the dwarf galaxy has a core density dominated by dark matter.

Dwarf galaxy	M_* [$M_\odot$]	$r_{1/2}$ [pc]	$\sigma_{v1\mathrm{D}}$ [km/s]	$v'_{h\mathrm{rms}}(1)/\sqrt{1-\kappa_h}$ [m/s]	ρ_{ch} [$10^6 M_\odot/\mathrm{kpc}^3$]
Antilla B	1×10^6	235 ± 27	8.0 ± 1.4	128 ± 12	43 ± 18
Aquarius	3×10^6	320 ± 27	7.8 ± 1.1	155 ± 11	22 ± 7
Cetus	5×10^6	575 ± 37	8.3 ± 1.0	234 ± 14	7.7 ± 2.1
IC 1613	2×10^8	1439 ± 57	10.8 ± 0.9	472 ± 18	2.1 ± 0.4
Leo A	1×10^7	365 ± 23	9.0 ± 0.6	178 ± 9	22 ± 4
Leo T	3×10^5	155 ± 24	7.5 ± 1.6	95 ± 12	87 ± 45
NGC 6822	3×10^8	1674 ± 187	23.2 ± 1.2	673 ± 51	7.1 ± 1.7
Pegasus dIrr	1×10^7	652 ± 42	12.3 ± 1.1	291 ± 15	13 ± 3
Phoenix	2×10^6	242 ± 20	9.3 ± 0.7	137 ± 8	55 ± 12
Sagittarius dIrr	9×10^6	259 ± 62	9.4 ± 1.1	143 ± 24	49 ± 26
Tucana	1×10^6	203 ± 38	6.2 ± 1.3	106 ± 15	34 ± 19
UGC 4879	1×10^7	301 ± 32	9.6 ± 1.2	160 ± 13	38 ± 12
WLM	9×10^7	754 ± 59	17.5 ± 2.0	360 ± 23	20 ± 6

Table 3. For some of the rotating dwarf galaxies, *i.e.* irregular dwarfs dIrr, in [7], we present the stellar mass M_*, neutral hydrogen mass M_{HI}, Wolf dynamical mass $M_{\mathrm{dyn}}(r_{1/2}) \equiv 930\sigma^2 r_{1/2}$, host galaxy, and half-light radius $r_{1/2}$. Data from the Local Volume Database [15]. Some entries are not available.

Dwarf	$\log_{10} M_*/M_\odot$	$\log_{10} M_{\mathrm{HI}}/M_\odot$	$\log_{10} M_{\mathrm{dyn}}/M_\odot$ to $r_{1/2}$	host	$r_{1/2}$ [pc]
DDO 126	8.13	8.03		no host	
DDO 133	8.39	8.25		no host	1709
DDO 154	7.96	8.28		no host	
NGC 2366	8.78	8.77		m 081	1436
NGC 3738	9.09	8.06		no host	
WLM	7.98	7.84	8.36	no host	799

5. Interpretation

It is interesting to compare the dwarf spheroidal dSph sample in the present study

(see Table 1 and Figures 1-5) with dwarfs in the Local Field (see Table 2) and with the rotating irregular dwarfs dIrr in [7] (some are included in Table 3). These three sets are not exclusive.

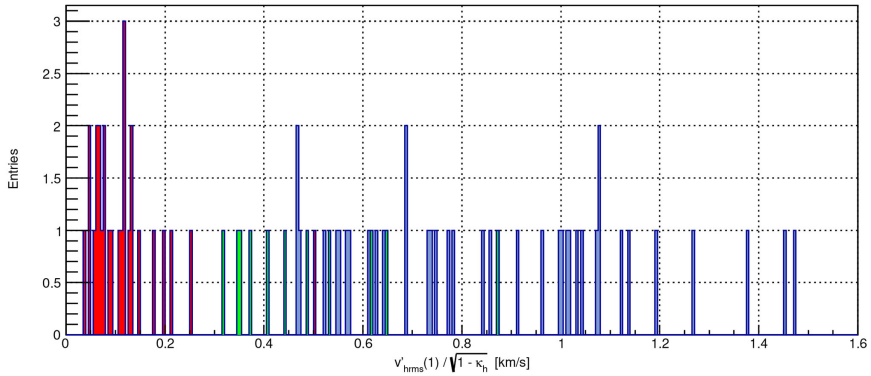

Figure 6. Measurements of $v'_{h\mathrm{rms}}(1)/\sqrt{1-\kappa_h}$. $v'_{h\mathrm{rms}}(1)$ is defined in (2). The distributions correspond to the spheroidal dwarfs dSph (see Figure 1 and Figure 2) (red), rotating irregular dwarfs dIrr from Figure 2 of [7] (green), and spiral galaxies from Figure 4 of [8] (blue).

Figure 6 compares the distributions of the measured $v'_{h\mathrm{rms}}(1)/\sqrt{1-\kappa_h}$ in the spheroidal dwarf dSph sample, with distributions for rotating irregular dwarfs dIrr in [7] and spiral galaxies in [8]. The spread in Figure 6 is due to dark matter rotation, relaxation and experimental uncertainties. The three distributions for $v'_{h\mathrm{rms}}(1)$ become approximately overlaid if $\kappa_h \approx 0$ for dSph, $\kappa_h \approx 0.82$ for dIrr, and $\kappa_h \approx 0.95$ for spirals. The remaining dispersion is due to dark matter relaxation, experimental uncertainties and residual rotation.

We have presented 27 measurements of $v'_{h\mathrm{rms}}(1)/\sqrt{1-\kappa_h}$, see Figures 1-5, and the distribution in Figure 6. We now present an interpretation of these measurements (that needs to pass the tests of independent observations). We interpret the dwarf spheroidal galaxies dSph with measured $v'_{h\mathrm{rms}}(1)/\sqrt{1-\kappa_h}$ in the range 45 to 131 m/s to be first-generation galaxies in the warm dark matter scenario, and to have little rotation. We note that 19 out of the 27 dwarf spheroidal galaxies have $v'_{h\mathrm{rms}}(1)/\sqrt{1-\kappa_h}$ in the range 45 to 131 m/s. The width of this distribution is due to relaxation, uncertainties of the observations, and residual rotation. With this interpretation, we obtain

$$\begin{aligned} v_{h\mathrm{rms}}(1) &= (\eta\epsilon/f)\cdot(88\pm 43)\,\mathrm{m/s},\\ k_{\mathrm{fs}} &= \big(f/(\eta\epsilon)\big)\cdot(10.4\mp 5.1)\,\mathrm{Mpc}^{-1},\\ m_{\mathrm{th}} &= (0.94\mp 0.42)\,\mathrm{keV}\ \text{ for } f/(\eta\epsilon)=0.5, \text{and}\\ m_h &= \big(f/(\eta\epsilon)\big)^{3/4}\cdot(0.65\mp 0.25)\,\mathrm{keV}\ \text{ for } N_b=1. \end{aligned} \tag{9}$$

$f=1$ if dark matter is collisional, or $f\approx\sqrt{3}$ if dark matter is collisionless [9]. For Andromeda XXI, $f\approx 1.13$ [4]. ϵ is the relaxation factor. m_h is obtained

from (20) with $N_b = 1$. If the dSph are first-generation warm dark matter galaxies, we may estimate $0.5 \lesssim \epsilon \lesssim 1$, including residual rotation, from the width of the distribution of $v'_{h\mathrm{rms}}(1)/\sqrt{1-\kappa_h}$. $\eta \approx 2.3$ is an estimate of the correction needed to account for the central black holes, see **Appendix C**.

In comparison with (9), the wavevector cut-off k_{fs} needed to understand the measured reionization optical depth, or the corresponding m_{th}, are $k_{\mathrm{fs}} = 2 \pm 1$ Mpc^{-1} [16] or $m_{\mathrm{th}} = 0.30 \pm 0.14$, or $m_{\mathrm{th}} = 0.51^{+0.22}_{-0.12}$ keV [18], or $1.30^{+0.30}_{-0.70}$ keV [19], or $0.66^{+0.07}_{-0.08}$ keV [19].

Assuming the number counts of dwarf galaxies in the Local Field are complete and of first generation, obtains $m_{\mathrm{th}} = 0.36^{+0.23}_{-0.26}$ keV [20][1].

Let us compare the measurement (9) with simulations in [21]. From Figure 8 of [21], the core radius in the two cases, $m_{\mathrm{th}} = 1.36$ and 0.52 keV, are 0.04 and 0.2 kpc. In comparison, the onset of the cores in **Figures 1-5** occurs in the range 0.2 to 0.6 kpc. So, this test favors the lower range of m_{th} and collisional dark matter.

Warm dark matter results in a cut-off of the galaxy mass distribution, so the smallest dwarf galaxies have dark-plus-baryon masses approximately 10^{11}, 10^{10} or $10^9 M_\odot$ for $m_{\mathrm{th}} = 0.25, 0.5$ or 1.0 keV, respectively (see Figure 4 of [22]). The smallest observed dwarfs in the Local Field have a dark matter mass, defined so $\langle \rho_h \rangle = 200 \Omega_m \rho_{\mathrm{crit}}$, of order 10^{10} to $10^9 M_\odot$ [20], corresponding to $0.5 \lesssim m_{\mathrm{th}} \lesssim 1.0$ keV.

The preceding comparisons favor collisional dark matter, with little relaxation (*i.e.* $\epsilon \approx 1$), and m_{th} near its lower range.

6. Conclusions

To obtain the dark matter "warmness", it is necessary to measure $v_{h\mathrm{rms}}(1)$ and k_{fs} in as many ways as possible. Here, we focus our attention on dark matter densities $\rho_h(r)$ of dwarf spheroidal galaxies dSph that have recently been measured thanks to observed line-of-sight velocities of individual stars. These dwarf spheroidals are dominated by dark matter. From observed densities $\rho_h(r)$ of 27 (mostly) dwarf spheroidal galaxies dSph, we estimate the results (9).

These results may be consistent, within uncertainties, with the observed optical depth due to reionization, with the number counts of dwarf galaxies in the Local Field, and with the observed masses of the smallest dwarf galaxies. However, the measurement (9) is in disagreement with published lower bounds on m_{th} that reach ≈10 keV (see summary in Figure 3 of [23]), while the Particle Data Group [24] sets model-independent lower bounds at ≈70 eV for fermion dark matter, and ≈10^{-22} eV for boson dark matter. These are pieces of a puzzle.

The case for degenerate dark matter is discussed in **Appendix D**.

The present measurement of $v_{h\mathrm{rms}}(1)$ and the independent measurement of k_{fs}

[1]In [20], we measured k_{fs}. We included a large correction due to the nonlinear re-generation of the small-scale density power spectrum. As a result of the present studies, I now believe that this correction should not be applied to first generation galaxies in the Local Field. Then we obtain $k_{\mathrm{fs}} \approx 5.6$ Mpc^{-1} and $m_{th} \approx 1$ keV.

in [20] are strong arguments in favor of warm dark matter. These measurements allow an extrapolation of the dark matter temperature to the past, suggesting a coupling of dark matter to a high-energy extension of the Standard Model of quarks and leptons, see **Appendix E**.

Acknowledgements

Some data in this article was obtained from the *Local Volume Database* (LVDB) catalog presented by Andrew B. Pace [15]. This catalog contains citations to each property of each dwarf galaxy, so a large community of astronomers has made the present investigation possible. I thank Karsten Müller for his early interest in this work and for many useful discussions.

Conflicts of Interest

The author declares no conflicts of interest regarding the publication of this paper.

References

[1] Yang, H., Wang, W., Zhu, L., Li, T.S., *et al.* (2025) The Dark Matter Content of Milky Way Dwarf Spheroidal Galaxies: Draco, Sextans and Ursa Minor. arXiv: 2507.02284.

[2] Pascale, R., Nipoti, C., Calura, F. and Della Croce, A. (2025) Leo I: The Classical Dwarf Spheroidal Galaxy with the Highest Dark Matter Density. *Astronomy & Astrophysics*, **700**, A77. https://doi.org/10.1051/0004-6361/202555004

[3] Pickett, C.S., Collins, M.L.M., Rich, R.M., Read, J.I., Charles, E.J.E., Martin, N., *et al.* (2025) Mass Modelling the Andromeda Dwarf Galaxies: Andromeda VI and Andromeda XXIII. *Monthly Notices of the Royal Astronomical Society*, **540**, 1701-1718. https://doi.org/10.1093/mnras/staf796

[4] Collins, M.L.M., Read, J.I., Ibata, R.A., Rich, R.M., *et al.* (2021) Andromeda XXI—A Dwarf Galaxy in a Low Density Dark Matter Halo. arXiv: 2102.11890.

[5] Charles, E.J.E., Collins, M.L.M., Rich, R.M., Read, J.I., *et al.* (2022) Andromeda XXV—A Dwarf Galaxy with a Low Central Dark Matter Density. arXiv: 2209.15022.

[6] Bezrukov, F., Gorbunov, D. and Koreshkova, E. (2025) Refining Lower Bounds on Sterile Neutrino Dark Matter Mass from Estimates of Phase Space Densities in Dwarf Galaxies. arXiv: 2412.20585.

[7] Hoeneisen, B. (2022) Measurement of the Dark Matter Velocity Dispersion with Dwarf Galaxy Rotation Curves. *International Journal of Astronomy and Astrophysics*, **12**, 363-381. https://doi.org/10.4236/ijaa.2022.124021

[8] Hoeneisen, B. (2019) The Adiabatic Invariant of Dark Matter in Spiral Galaxies. *International Journal of Astronomy and Astrophysics*, **9**, 355-367.

[9] Hoeneisen, B. (2025) Warm Dark Matter Studies with Spiral Galaxy Data. *International Journal of Astronomy and Astrophysics*, **15**, 336-355. https://doi.org/10.4236/ijaa.2025.154021

[10] Hoeneisen, B. (2024) Understanding Elliptical Galaxies with Warm Dark Matter. *Physics of the Dark Universe*, **46**, Article ID: 101643. https://doi.org/10.1016/j.dark.2024.101643

[11] Hoeneisen, B. (2025) The Warm Dark Matter Plus Baryon Linear Power Spectrum. *International Journal of Astronomy and Astrophysics*, **15**, 264-281. https://doi.org/10.4236/ijaa.2025.153017

[12] Boyanovsky, D., de Vega, H.J. and Sanchez, N.G. (2008) Dark Matter Transfer Function: Free Streaming, Particle Statistics, and Memory of Gravitational Clustering. *Physical Review D*, **78**, Article ID: 063546. https://doi.org/10.1103/physrevd.78.063546

[13] Viel, M., Lesgourgues, J., Haehnelt, M.G., Matarrese, S. and Riotto, A. (2005) Constraining Warm Dark Matter Candidates Including Sterile Neutrinos and Light Gravitinos with WMAP and the Lyman-α Forest. *Physical Review D*, **71**, Article ID: 063534. https://doi.org/10.1103/physrevd.71.063534

[14] Hoeneisen, B. (2024) Measurements of the Dark Matter Mass, Temperature and Spin. *International Journal of Astronomy and Astrophysics*, **14**, 184-202. https://doi.org/10.4236/ijaa.2024.143012

[15] Pace, A.B. (2025) The Local Volume Database: A Library of the Observed Properties of Nearby Dwarf Galaxies and Star Clusters. arXiv: 2411.07424.

[16] Hoeneisen, B. (2022) Measurement of the Dark Matter Velocity Dispersion with Galaxy Stellar Masses, UV Luminosities, and Reionization. *International Journal of Astronomy and Astrophysics*, **12**, 258-272. https://doi.org/10.4236/ijaa.2022.123015

[17] Hoeneisen, B. (2025) Why Do Galaxies Have Extended Flat Rotation Curves? *International Journal of Astronomy and Astrophysics*, **15**, 1-10. https://doi.org/10.4236/ijaa.2025.151001

[18] Lin, H., Gong, Y., Yue, B. and Chen, X. (2023) Implications of the Stellar Mass Density of High-z Massive Galaxies from JWST on Warm Dark Matter. *Research in Astronomy and Astrophysics*, **24**, Article ID: 015009. https://doi.org/10.1088/1674-4527/ad0864

[19] Lapi, A., Ronconi, T., Boco, L., Shankar, F., Krachmalnicoff, N., Baccigalupi, C., *et al.* (2022) Astroparticle Constraints from Cosmic Reionization and Primordial Galaxy Formation. *Universe*, **8**, Article 476. https://doi.org/10.3390/universe8090476

[20] Hoeneisen, B. (2026) Estimate of the Warm Dark Matter Free-Streaming Cut-Off with Isolated Dwarf Galaxies in the Local Field. *International Journal of Astronomy and Astrophysics*, **16**, 11-24. https://doi.org/10.4236/ijaa.2026.161002

[21] Macciò, A.V., Paduroiu, S., Anderhalden, D., Schneider, A. and Moore, B. (2012) Cores in Warm Dark Matter Haloes: A Catch 22 Problem. *Monthly Notices of the Royal Astronomical Society*, **424**, 1105-1112. https://doi.org/10.1111/j.1365-2966.2012.21284.x

[22] Schneider, A., Smith, R.E. and Reed, D. (2013) Halo Mass Function and the Free Streaming Scale. *Monthly Notices of the Royal Astronomical Society*, **433**, 1573-1587. https://doi.org/10.1093/mnras/stt829

[23] Liu, B., Shan, H. and Zhang, J. (2024) New Galaxy UV Luminosity Constraints on Warm Dark Matter from JWST. *The Astrophysical Journal*, **968**, Article 79. https://doi.org/10.3847/1538-4357/ad4ed8

[24] Navas, S., *et al.* (2024) The Review of Particle Physics. *Physical Review D*, **110**, Article ID: 030001.

[25] Hoeneisen, B. (2019) A Study of Dark Matter with Spiral Galaxy Rotation Curves. *International Journal of Astronomy and Astrophysics*, **9**, 71-96. https://doi.org/10.4236/ijaa.2019.92007

[26] Hoeneisen, B. (2022) Warm Dark Matter and the Formation of First Galaxies. *Journal of Modern Physics*, **13**, 932-948. https://doi.org/10.4236/jmp.2022.136053

[27] Chavanis, P. (2022) Predictive Model of Fermionic Dark Matter Halos with a Quantum Core and an Isothermal Atmosphere. *Physical Review D*, **106**, Article ID: 043538. https://doi.org/10.1103/physrevd.106.043538

Appendix

A. Galaxy Rotation

Let us consider galaxy rotation. The equations are [25]

$$\nabla \cdot \boldsymbol{g}_b = -4\pi G\rho_b, \quad \nabla \cdot \boldsymbol{g}_h = -4\pi G\rho_h, \tag{10}$$

$$\boldsymbol{g} = \boldsymbol{g}_b + \boldsymbol{g}_h, \quad g_b \equiv -\frac{V_b^2}{r}, \quad g_h \equiv -\frac{V_h^2}{r}, \quad V^2 \equiv V_b^2 + V_h^2, \tag{11}$$

$$\nabla P_b = \rho_b\left(\boldsymbol{g} + \kappa_b(r)\frac{V^2}{r}\hat{\boldsymbol{e}}_r\right), \quad \nabla P_h = \rho_h\left(\boldsymbol{g} + \kappa_h(r)\frac{V^2}{r}\hat{\boldsymbol{e}}_r\right), \tag{12}$$

$$P_b = \left\langle v_{rb}^2\right\rangle \rho_b \quad \text{and} \quad P_h = \left\langle v_{rh}^2\right\rangle \rho_h. \tag{13}$$

$V(r)$ is the circular rotation velocity of a test particle, with contributions in quadrature $V_h(r)$ and $V_b(r)$ from dark matter and baryons, respectively. $\kappa_h(r)$ and $\kappa_b(r)$ measure the rotation of dark matter and baryons. For simplicity, we take κ_h and κ_b to be independent of r. Note that $\left\langle v_{rh}^2\right\rangle$ appears in the combination $\left\langle v_{rh}^2\right\rangle / (1-\kappa_h)$.

B. A Study of the Effect of Baryons

A study of the effect of baryons in Leo I is presented in **Figure A1**.

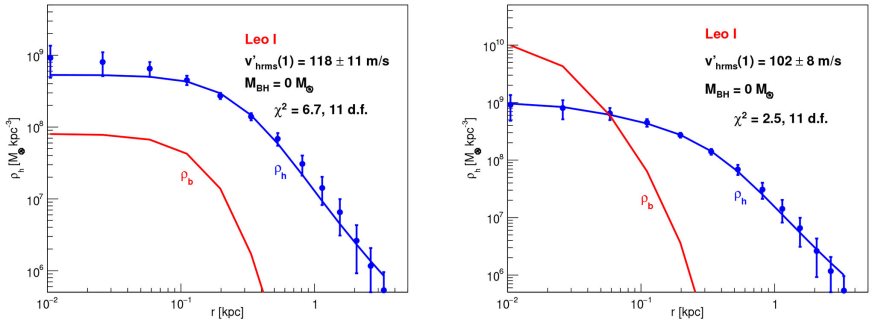

Figure A1. Dark matter density $\rho_h(r)$ and baryon density $\rho_b(r)$ of Leo I. The left figure has fixed $\rho_b(10\,\text{pc}) = 8\times10^7 M_\odot \cdot \text{kpc}^{-3}$, and obtains $v'_{h\text{rms}}(1) = 118 \pm 11$ (stat) m/s. The right figure has fixed $\rho_b(10\,\text{pc}) = 1\times10^{10} M_\odot \cdot \text{kpc}^{-3}$, and obtains $v'_{h\text{rms}}(1) = 102 \pm 8$ (stat) m/s. The continuous lines are integrations of hydrostatic equations of dark matter plus baryons (see **Appendix A**). Only the dark matter $\rho_h(r_i)$ is fit.

C. Correction η Due to the Central Black Hole

All fits in **Figures 1-5** have $v'_{h\text{rms}}(1)$ defined in (2) with $\rho_h(r_{\min})$ being the dark matter density of the first measured point in the figures. Equation (2) assumes a cored isothermal sphere, *i.e.* neglects a possible central black hole. Due to a black hole, the distribution $\rho_h(r)$ departs from a cored isothermal sphere, and the resulting fit of $v'_{h\text{rms}}(1)/\sqrt{1-\kappa_h}$ becomes dependent on the first measured $\rho_h(r_{\min})$. Omitting the first measurement presented in the figures results in a shift of the meaured $v'_{h\text{rms}}(1)/\sqrt{1-\kappa_h}$ by ≈+14%, or $\approx +1\sigma$.

The question then is how to proceed if there is a central black hole?

The formation of the cored isothermal sphere starting from a Gaussian initial perturbation was studied in [26] for collisional dark matter. For a given $\langle v_{rh}^2 \rangle$, the core density ρ_{ch} is determined by the adiabatic invariant $v_{h\mathrm{rms}}(1)$. The formation of a black hole will then change $\rho_h(r)$. To estimate the uncertainty due to the black hole, an alternative analysis would use r_4 (at the onset of the core and where the uncertainty of $\rho_h(r_i)$ is near its minimum) instead of the first measured radius $r_{\min} \equiv r_0$, see **Figures 1-5**. With r_4, the result $v'_{h\mathrm{rms}}(1)/\sqrt{1-\kappa_h}$ becomes insensitive to the first measurement or to the black hole mass M_{BH}. This change from r_0 to r_4 results in replacing $\eta = 1$ in (9) by $\eta \approx 2.3$.

D. Degenerate Dark Matter in Dwarf Spheroidal Galaxies?

We consider fermion dark matter with spin 1/2, *i.e.* $N_f = 2$, and compare the central pressure of a non-degenerate gas

$$P = \frac{1}{3} v_{h\mathrm{rms}}^2(1) \rho_c \left(\frac{\rho_c}{\Omega_c \rho_{\mathrm{crit}}} \right)^{2/3}, \tag{14}$$

with the central pressure of a fully degenerate Fermi gas

$$P_F = \frac{\left(3\pi^2 \hbar^3\right)^{2/3}}{5 m_h} \left(\frac{\rho_c}{m_h} \right)^{5/3}. \tag{15}$$

Consider Leo I with $v'_{h\mathrm{rms}}(1) = 115$ m/s, $\rho_c = 9 \times 10^8 \, M_\odot / \mathrm{kpc}^3$ and, for example, $m_h = 442$ eV, see **Figure 1** and (9). For Leo I, we obtain $P = 2.4 \times 10^{-11}$ N/m^2 and $P_F = 3.8 \times 10^{-12}$ N/m^2, so there is onset of degeneracy in the core of this galaxy if dark matter is fermionic. For a full treatment of fermion dark matter in dwarf galaxies, see [27].

E. Journey to the Past

For non-relativistic non-degenerate dark matter,

$$\frac{1}{2} m_h \langle v_h^2 \rangle = \frac{3}{2} k T_h. \tag{16}$$

$a_{\mathrm{NR}} \equiv v_{h\mathrm{rms}}(1)/c$ is the expansion parameter at which dark matter becomes non-relativistic. The number density of ultra-relativistic dark matter, assumed to have zero chemical potential, is [24]

$$n = \frac{\zeta(3)}{\pi^2} \left(\frac{k T_h}{\hbar c} \right)^3 \left\{ N_b + \frac{3}{4} N_f \right\}, \tag{17}$$

with $\zeta(3)/\pi^2 \approx 0.1218$. In this Appendix, we neglect threshold effects. At $a = a_{\mathrm{NR}}$,

$$n = \frac{\Omega_c \rho_{\mathrm{crit}}}{m_h a_{\mathrm{NR}}^3}. \tag{18}$$

From the preceding equations

$$m_h = \left(\frac{27\hbar^3 \Omega_c \rho_{\text{crit}}}{0.1218 \cdot v_{h\text{rms}}(1)^3 \left(N_b + \frac{3}{4} N_f \right)} \right)^{1/4}. \tag{19}$$

For boson dark matter,

$$m_h = 107.3 \text{ eV} \left(\frac{760 \text{ m/s}}{v_{h\text{rms}}(1)} \right)^{3/4} N_b^{-1/4}. \tag{20}$$

For fermion dark matter,

$$m_h = 115.3 \text{ eV} \left(\frac{760 \text{ m/s}}{v_{h\text{rms}}(1)} \right)^{3/4} N_f^{-1/4}. \tag{21}$$

(We have kept the "760 m/s" to ease comparison with [14].)

Let a_{dec} be the expansion parameter at which dark matter decouples from the (extended) Standard Model of quarks and leptons. Define $g'_h \equiv \left(N_b + \frac{7}{8} N_f \right)$ for the dark matter, and $g_{\text{dec}} \equiv \sum \left(N_b + \frac{7}{8} N_f \right)$ for the (extended) Standard Model at a_{dec}. At a_{dec}, all particles have the same temperature $T_{h\text{dec}}$, and the entropy per unit comoving volume is [24]

$$s = \frac{2\pi^2}{45} \left(\frac{k T_{h\text{dec}} a_{\text{dec}}}{\hbar c} \right)^3 \left(g'_h + g_{\text{dec}} \right). \tag{22}$$

Note that $T_{h\text{dec}} a_{\text{dec}} = T_{h\text{NR}} a_{\text{NR}}$. At a_{NR} the entropy per unit comoving volume has contributions from dark matter, photons, and neutrinos:

$$s = \frac{2\pi^2}{45} \left(\frac{k T_{h\text{dec}} a_{\text{dec}}}{\hbar c} \right)^3 \left(g'_h + \left(\frac{T_{\gamma\text{NR}}}{T_{h\text{NR}}} \right)^3 \left\{ 2 + \frac{7 \times 6}{8 \times 1.40^3} \right\} \right). \tag{23}$$

$T_{\gamma\text{NR}} = T_{\gamma 0} / a_{\text{NR}} = T_{\gamma 0} c / v_{h\text{rms}}(1)$ and $T_{h\text{NR}} = m_h c^2 / (3k)$, so

$$\frac{T_{h\text{NR}}}{T_{\gamma\text{NR}}} = \frac{0.386}{N_b^{1/4}} \left(\frac{v_{h\text{rms}}(1)}{760 \text{ m/s}} \right)^{1/4}, \tag{24}$$

for boson dark matter, and

$$\frac{T_{h\text{NR}}}{T_{\gamma\text{NR}}} = \frac{0.415}{N_f^{1/4}} \left(\frac{v_{h\text{rms}}(1)}{760 \text{ m/s}} \right)^{1/4}, \tag{25}$$

for fermion dark matter. We note that dark matter is sufficiently cold not to upset Big-Bang nucleosynthesis [24]. Conservation of entropy then obtains

$$g_{\text{dec}} = 68.0 \left(\frac{760 \text{ m/s}}{v_{h\text{rms}}(1)} \right)^{3/4} N_b^{3/4} \tag{26}$$

for boson dark matter, and

$$g_{\text{dec}} = 54.8 \left(\frac{760 \text{ m/s}}{v_{h\text{rms}}(1)} \right)^{3/4} N_f^{3/4} \tag{27}$$

for fermion dark matter.

For comparison, we consider the case of scalar dark matter coupled to the Higgs boson, and in thermal and diffusive equilibrium with the relativistic Higgs boson, *i.e.* $N_b = 1$ and $g_{\text{dec}} = 95.25$. For this case, $v_{h\text{rms}}(1) = 679$ m/s and $k_{\text{fs}} = 1.0$ Mpc^{-1}. Since the measured $v_{h\text{rms}}(1)$ is less than 679 m/s, the suggestion is that dark matter couples to a high-energy extension of the Standard Model of quarks and leptons.